DOI: 10.1021/ma101250e

Macromolecules
ARTICLE

Phase Behavior of Off-Critical A/B/A−C Blends

Alisyn J. Nedoma,[†] Peggy Lai,[†] Andrew Jackson,[‡,§] Megan L. Robertson,[†] and Nitash P. Balsara*[,†,∥,⊥]

[†]*Department of Chemical Engineering, University of California, Berkeley, California 94720,*
[‡]*National Institute of Standards and Technology Center for Neutron Research, Gaithersburg, Maryland 20899,*
[§]*Department of Materials Science and Engineering, University of Maryland, College Park, Maryland 20742,*
[∥]*Materials Sciences Division, Lawrence Berkeley National Laboratory, Berkeley, California 94720, and*
[⊥]*Environmental Energy Technologies Division, Lawrence Berkeley National Laboratory, Berkeley, California 94720*

Received June 4, 2010; Revised Manuscript Received August 1, 2010

ABSTRACT: Small-angle neutron scattering (SANS) was used to study the phase behavior of A/B/A−C blends wherein A and B were immiscible homopolymers and A−C was an amphiphilic diblock copolymer. A series of blends were prepared with a fixed diblock copolymer volume fraction of 0.40, and the volume fraction of A homopolymer was varied from 0.1 to 0.5. All blends exhibited the same quantitative phase behavior despite differences in blend composition: lamellae below 115 °C and macrophase separation above 122 °C. Least-squares fits of the SANS data below 115 °C were used to extract information about the A-rich and B-rich lamellae using a model for randomly oriented lamellae developed by Hosemann and Bagchi. Our approach explicitly accounts for the concentration fluctuations within the lamellae using the random phase approximation. The results of the analysis were found to agree with predictions calculated using self-consistent-field theory (SCFT) with no adjustable parameters. The experimentally determined transitions from lamellae to macrophase separation were also in good agreement with SCFT. Calculations based on multicomponent RPA predicted a small homogeneous window that was not experimentally observed in any of the blends studied.

Introduction

Diblock copolymers have been added to binary blends of immiscible homopolymers to induce the formation of stable microstructures[1−29] as predicted by mean-field theories.[3,30−48] Analogous to oil/water/nonionic surfactant systems, the polymer blends that we have studied comprise immiscible A and B homopolymers (the analogues of oil and water phases) and an amphiphilic A−C diblock copolymer (analogue of the nonionic surfactant).[49−52] In previous studies, we have reported on the effect of adding A−C copolymers to a series of binary blends of A and B homopolymers at the critical composition.[21−29] We use the Flory−Huggins theory to obtain the critical composition:[53,54]

$$\phi_{A,crit} = \frac{1}{1+(N_A/N_B)^{1/2}} \quad (1)$$

Most of our previous studies on A/B/A−C blends were restricted to cases where $N_A \approx N_B$, i.e., $\phi_{A,crit} \approx 0.5$. In a more recent study we explored critical blends wherein $N_A \neq N_B$.[29]

The present paper represents our first study of A/B/A−C blends wherein the A−C copolymer is added to off-critical blends of A and B homopolymers. Experimental data obtained from SANS were compared with theoretical predictions of the phase behavior for these blends. Mean-field theories were used with previously measured binary Flory−Huggins interaction parameters and statistical segment lengths.[23,27,55] As in previous studies,[23,24,27,29] we used the SANS profiles to determine the phase behavior of the blends.

*To whom correspondence should be addressed: e-mail nbalsara@berkeley.edu; Ph 510.642.8937; Fax 510.642.4778.

Experimental Methods

The experimental system chosen for this work has been described in previous publications.[23−29] Species A and C were both saturated polybutadienes where A contained 89% 1,2-addition of the butylene monomer and C contained 63% 1,2-addition. Component A was partially deuterated for neutron contrast, and component C was hydrogenated. They were both synthesized by anionic polymerization (the A-C copolymer was synthesized by sequential anionic polymerization) and then saturated using a pressure reactor. Component B, polyisobutylene, was synthesized by cationic polymerization. The synthesis and characterization[56] of these materials are described in refs 23 and 27. The polymers used in this study are listed in Table 1. The A homopolymer was nearly 2/3 the length of the B homopolymer ($N_A/N_B = 0.60$, and $\phi_{A,crit} = 0.564$ by eq 1), and the diblock copolymer was nearly symmetric with the volume fraction of A in the copolymer, $f_A = 0.55$. We use the symbol N_i to refer to the chain length of species i based on a reference volume of 0.1 nm^3. The chain lengths of the homopolymers and diblock copolymer were chosen to lie nominally within the wet brush regime ($N_A/N_{A-C} = 0.17$, $N_B/N_{A-C} = 0.28$). This is a regime wherein the homopolymer chain lengths are substantially smaller than that of the copolymer, and this enables penetration of the homopolymer chains into the diblock copolymer brush that lies between the A-rich and B-rich microphases.[10,13,31,57]

The compositions of the blends examined are listed in Table 2 where $\phi_A + \phi_B + \phi_{diblock} = 1$. The volume fraction of diblock copolymer was held constant at $\phi_{diblock} = 0.40$. Details of the blending process are given in refs 23 and 29. The eight off-critical blends are named OC*XX*, where *XX* is the percent of A homopolymer in the blend; the critical blend is named TB0.6 (ternary blend, $N_A/N_B = 0.6$) for consistency with a previous reference[29] (see Table 2). The total bulk fraction of component A in a blend,

 Published on Web 08/30/2010 © 2010 American Chemical Society

$\phi_{A,TOT}$ in Table 2, is the sum of contributions from the A homopolymer and the A-block of the copolymer.

Small-angle neutron scattering (SANS) measurements were made at the NG3 and NG7 beamlines at the National Institute of Standards and Technology Center for Neutron Research in Gaithersburg, MD. Samples were placed into the beamline at room temperature and heated incrementally from 30 to 190 °C. Each temperature step was followed by a 10 min anneal to allow the samples to equilibrate; previous work with this system has shown that this amount of time is sufficient to obtain reproducible SANS profiles that do not vary with time.[23−25,27,29] Six of the blends (those with $\phi_A = 0.1-0.338$) were heated a second time from 110 to 130 °C in 2 °C increments to more accurately determine the temperatures of the phase transitions. These runs included a 5 min anneal after each temperature step, shown to be adequate for equilibration after small temperature steps. SANS data were corrected for background, empty cell, transmission, corrections for scattering contributions due to nonuniform deuteration,[58] and integrated azimuthally to render coherent scattering intensity, I, versus magnitude of the scattering vector, q, profiles ($q = 4\pi \sin(\theta/2)/\lambda$ in which θ is the scattering angle and λ is the wavelength of incident neutrons).[59] The measured SANS profiles were compared with model predictions that were convoluted ("smeared") with the instrument resolution function provided by NIST.[59] The smeared models agreed quantitatively with the SANS data, while unsmeared models did not capture the widths of scattering peaks within the microphase-separated window.

Results and Discussion

SANS profiles at selected temperatures are shown for blend OC40 in Figure 1a. At 30 °C, the blend exhibits a primary scattering peak at $q = q^*$, and a higher order scattering peak at $q = 2q^*$, consistent with the scattering expected from a lamellar phase. The lamellar phase persists in blend OC40 as the sample temperature is increased until 120 °C. At higher temperatures the SANS profiles exhibit an upturn in the low-q scattering, indicating the onset of macrophase separation. The SANS profiles at 130 and 170 °C show a broad correlation peak at finite q in addition to low q upturn at low q, suggesting that one of the coexisting macrophases is microphase-separated, a phenomenon previously documented by several groups.[14,21,29] Surprisingly, we found that the SANS profiles for all nine blends listed in Table 2 were qualitatively similar to Figure 1: at low temperatures there was a peak at finite q, and above 130 °C there was an upturn in the low-q scattering intensity. We do not show these profiles for brevity.

We measured SANS profiles while heating and cooling blend OC40 in the temperature window of 90−130 °C. The profiles overlapped from the heating and cooling runs, suggesting equilibrium behavior at each temperature. However, the profiles obtained for different thermal histories varied slightly in the intensity and sharpness of the peaks while retaining the same qualitative features and primary peak locations. This is not surprising as the widths of the SANS peaks are related to factors such as the extent of long-range order (in the case of ordered microphases) which is known to depend on thermal history.

Table 1. Polymer Characterization

polymer species	M_w,[a] kg/mol	N_i[b]	PDI	ρ,[c] g/cm^3 (at 23 °C)	n_D
dPBD	25.3	463	1.01	0.9070	2.79
PIB	42.5	772	1.04	0.9135	
HPBD−hPBD	78.5−65.4	1509−1257	1.01	0.8639	

[a] GPC measurements were used to determine M_w, the weight-averaged molecular weight, and PDI, the polydispersity index. [b] N_i is the number of reference volumes, v_0, comprising a polymer chain where $v_0 = 0.1$ nm^3. [c] A methanol/ethylene glycol density gradient column was used to measure the density, ρ, of all species. ρ was used to calculate the average number of deuterium atoms per monomer unit, n_D, for the deuterated polybutadiene homopolymers.

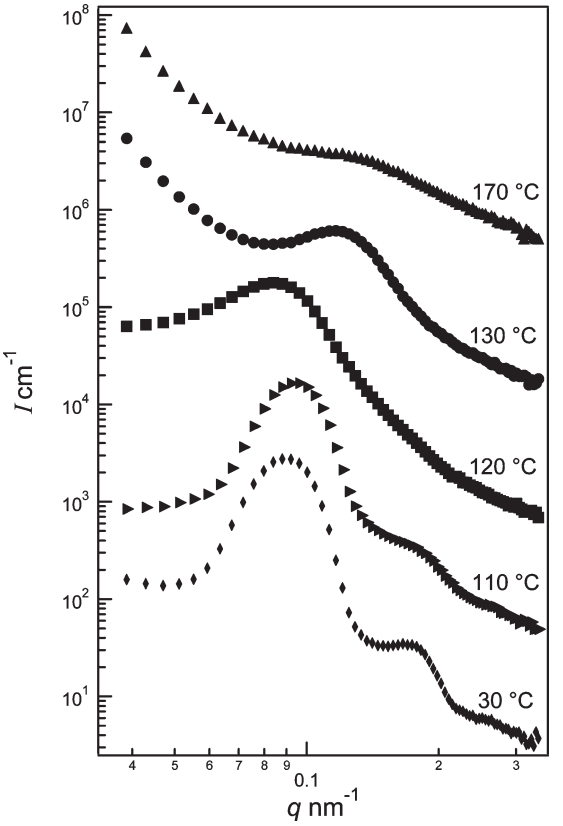

Figure 1. SANS intensity, I, versus scattering vector, q, at selected temperatures for blend OC40. Thermal history is 1 h anneal time at 90 °C and slow cooling to room temperature. Profiles have been shifted vertically as follows: 30 °C (0 cm^{-1}), 110 °C (1.5×10^8 cm^{-1}), 120 °C (3.0×10^8 cm^{-1}), 130 °C (4.8×10^8 cm^{-1}), 170 °C (6.8×10^8 cm^{-1}).

Table 2. Characterization of Blends Studied

blend	ϕ_A	$\phi_{A,TOT}$	$\phi_{A\text{-dom}}$[b]	d (nm)[b]	σ_A (nm)[b]	σ_B (nm)[b]
OC10	0.100	0.318	0.359−0.431	59.9−74.7	0.995−5.44	6.27−12.2
OC15	0.150	0.368	0.233−0.587	62.3−73.5	5.38−8.37	0.880−12.3
OC20	0.200	0.418	0.297−0.357	63.2−74.2	1.96−9.04	5.06−11.9
OC25	0.250	0.468	0.346−0.398	62.9−67.9	2.78−4.89	4.75−8.49
OC30	0.300	0.518	0.587−0.636	63.2−76.2	5.19−17.0	2.46−5.84
TB0.6[a]	0.338*	0.556	0.573−0.612	62.4−66.9	3.90−8.41	2.16−5.11
OC40	0.400	0.618	0.599−0.621	64.7−70.6	6.40−12.5	1.92−4.60
OC45	0.450	0.668	0.575−0.586	60.2−68.0	5.99−6.51	1.21−2.13
OC50	0.500	0.718	0.567−0.600	56.4−67.2	5.39−7.88	1.23−2.46

[a] The name TB0.6 is chosen to agree with ref 29. [b] These parameters indicate the ranges found by fitting SANS data with eq 3. * The asterisk denotes the blend that is prepared at the Flory−Huggins critical composition with respect to the copolymer-free binary blend.

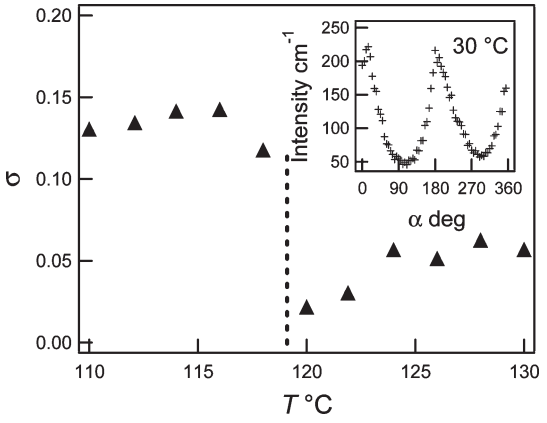

Figure 2. Standard deviation, σ, of the SANS profiles integrated between $q = 0.07$ and 0.12 nm^{-1} versus temperature for blend OC25. The inset shows the integrated intensity versus azimuthal angle, α, at 30 °C.

All of the samples exhibited azimuthally asymmetric scattering in the temperature window from 30 to ~120 °C. The presence of azimuthal asymmetry has been shown to result from the alignment of anisotropic microstructures during sample preparation.[60,61] Following previous work,[29] the integrated SANS intensity between $q = 0.07$ and 0.12 nm^{-1}, in the vicinity of the primary peak, was determined as a function of azimuthal angle, α, and the standard deviation of the data set, σ, was taken as a measure of azimuthal asymmetry. The results of this integration, obtained for OC25 at 30 °C, are shown in the inset of Figure 2, giving $\sigma = 0.471$. The temperature dependence of σ for blend OC25 is also shown in Figure 2. There is a sharp decrease in σ between 118 and 120 °C, in good agreement with the onset of macrophase separation inferred from the upturn in the low-q scattering data. The σ-based measurement of the transition temperature from anisotropic to isotropic scattering was found to agree with the onset of macrophase separation for all blends studied.

The presence of a single scattering peak can, in principle, indicate the presence of a weakly ordered lamellar phase or a microemulsion. The intensity predicted by the Teubner−Strey equation for microemulsions, $I_{\mu E}$, is given by[62]

$$I_{\mu E}(q) = \frac{1}{a + bq^2 + cq^4} \tag{2}$$

where the fitting parameter b is of particular interest as it is negative for the case of microemulsions.

The scattering profile from randomly oriented lamellae, I_{lam}, is given by[63]

$$I_{lam}(q) = \frac{C}{q^4} f(q) \tag{3}$$

where C is a constant that is related to the number of lamellae in the scattering volume and the average scattering contrast between the lamellae, and the function $f(q)$ is given by[64,65]

$$\begin{aligned} f(q) = {} & [(1-g_A)(1-g_B)(1-g_A g_B) \\ & + 2g_A(1-g_B^2)\sin^2(q\phi_{A\text{-dom}}/2) \\ & + 2g_B(1-g_A^2)\sin^2(q\phi_{B\text{-dom}}/2)]/[(1-g_A g_B)^2 \\ & + 4g_A g_B \sin^2(qd/2)] \end{aligned} \tag{4}$$

where

$$g_A = e^{-(1/2)\sigma_A^2 q^2}, \quad g_B = e^{-(1/2)\sigma_B^2 q^2}$$

The parameters $\phi_{A\text{-dom}}$ and $\phi_{B\text{-dom}}$ refer to the volume fractions of the A-rich and B-rich lamellae ($\phi_{A\text{-dom}} + \phi_{B\text{-dom}} = 1$), d is the average overall domain spacing (the center-to-center distance between adjacent A-rich lamellae), and the widths of the A and B lamellae are assumed to follow a Gaussian distribution with a variance of σ_A and σ_B. We ignore the fact that the lamellae in our samples are not randomly oriented (Figure 2). The SANS intensity profiles are fit with five adjustable parameters: C, σ_A, σ_B, d, and $\phi_{A\text{-dom}}$.

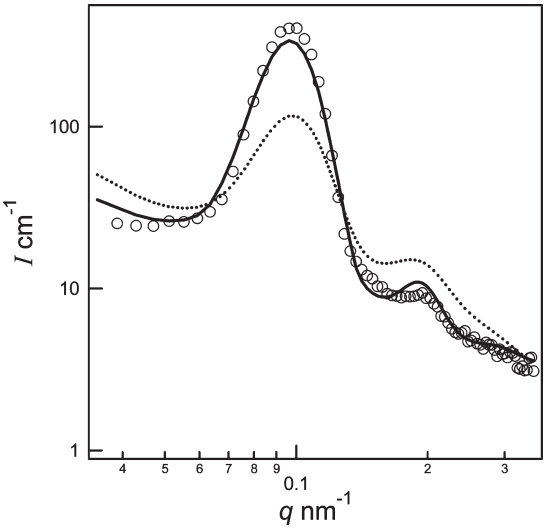

Figure 3. SANS intensity, I, versus scattering vector, q, for blend OC25 at 30 °C (○). The dashed curve is a fit of $I_{lam}(q)$ (eq 3). Full curve is a fit of $I_{lam} + I_{A,fluc}$ (eq 8).

The dashed curve in Figure 3 represents the least-squares fit of $I_{lam}(q)$ to $I(q)$ obtained from OC25 at 30 °C. It is evident that the model is inconsistent with the SANS data. One of the difficulties with the expression for I_{lam} is that it is based on the assumption that the microphases themselves are unstructured. In our A/B/A−C mixtures the A-rich domains comprise primarily of the homopolymer dPBD and the hPBD block belonging to the HPBD−hPBD diblock copolymer (see Table 2). The scattering due to concentration fluctuations in the A-rich microdomains, $I_{A,fluc}$, is expected to contribute to the measured SANS intensity. We use the RPA to compute scattering from fluctuations of the chains in the A-rich domains:

$$\begin{aligned} I_{A,fluc}(q) = {} & B^2\left(\frac{1}{N_{hPBD} v_{hPBD} \phi_{hPBD} P_{hPBD}(q)}\right. \\ & \left. + \frac{1}{N_{dPBD} v_{dPBD} \phi_{dPBD} P_{dPBD}(q)}\right)^{-1} \end{aligned} \tag{5}$$

where B is the scattering contrast, related to the scattering length of species i, b_i, and monomer volume, v_i, as

$$B = \frac{b_{hPBD}}{v_{hPBD}} - \frac{b_{dPBD}}{v_{dPBD}} \tag{6}$$

$P_i(q)$ is the Debye function for species i:

$$P_i(q) = 2\frac{\exp(-x_i) + x_i - 1}{x_i^2} \tag{7}$$

and $x_i = R_{g,i}^2 q^2$. The radius of gyration is given by $R_{g,i}^2 = N_i l_i^2/6$, where l_i is the statistical segment length, given for each species in footnote 66. Equation 5 is based on the assumption of ideal mixing (i.e., $\chi = 0$ between hPBD/dPBD) in the A-rich domains. Self-consistent-field theory calculations are used below to predict concentration profiles in the A-rich domains. The proposed corrections (eqs 5−7), which accounts for chain connectivity

only, represent the simplest possible approach. Self-consistent-field theory calculations described below will show that many complexities of the system are unaccounted for in our approach. The proposed approach does not introduce additional fitting parameters. We assume, for simplicity, that the measured SANS intensity is simply a linear sum of contributions from the lamellar structure factor and the concentration fluctuations term; i.e., the total scattering is an incoherent sum of the two individual contributions.

$$I(q) = I_{\text{lam}}(q) + I_{\text{A, fluc}}(q) \tag{8}$$

In eq 8, we neglect the contributions due to concentration fluctuations in the B-rich lamellae. The value of $I_{\text{B,fluc}}$ is estimated to be 2 orders of magnitude less than that of $I_{\text{A,fluc}}$ because both B and C chains are hydrogenated, with nearly identical scattering length densities. Note that both the fits shown in Figure 3 have the same number of fitting parameters, listed in Table 3 for both fits. It is clear that accounting for the fluctuations within the lamellae leads to a significant reduction in the deviation between the model and experiments. We tried fitting $I(q)$ with $I_{\mu\text{E}}(q)$ but found large discrepancies between the model and experiments. Our analysis based on the lamellar structure factor leads to the conclusion that OC25 at 30 °C forms a lamellar microphase.

One may argue that detailed fitting of the lamellar structure factor was unnecessary for proving that OC25 at 30 °C forms a lamellar phase due to the presence of a shoulder at $q = 2q^*$. There are, however, several SANS profiles that only contained a primary peak. An example of this is shown in Figure 4 where we show $I(q)$ of OC10 at selected temperatures. A single scattering peak is seen at 30 °C. The profiles at 30 and 124 °C were obtained from the first SANS run after annealing the sample at 90 °C, while the profiles at 110, 118, and 122 °C were obtained from the second SANS run after annealing the sample at 190 °C. Figure 4a shows fits of $I_{\text{lam}}(q)$ through the data while in Figure 4b we show the fits of $I_{\mu\text{E}}(q)$ through the same data set. It is evident that the $I_{\text{lam}}(q)$ fits through $I(q)$ are significantly better than those of $I_{\mu\text{E}}(q)$. The $I_{\text{lam}}(q)$ fits are consistent with the data when there is only one primary peak as is the case at 30 °C, as well as cases when both a primary peak and a shoulder at $2q^*$ are present, as is the case at 116 °C (Figure 4a). We thus conclude that a lamellar phase is obtained in OC10 at temperatures ≤120 °C.

The fitted parameters obtained from sample OC10 at selected temperatures are given in Table 4 for the $I_{\text{lam}}(q)$ fits and Table 5 for the $I_{\mu\text{E}}(q)$ fits (shown for completeness). The SANS profile for OC10 at 110 °C was measured during both runs and allows us to compare the effects of thermal history on the fitting parameters. We find that the domain spacings and σ values are similar for both thermal histories. The fitted value of $\phi_{\text{A-dom}}$ is larger for the high temperature anneal, and for both annealing temperatures $\phi_{\text{A-dom}}$ is somewhat larger than the bulk value of component A in the blend, $\phi_{\text{A,TOT}} = 0.318$. The values of $\sigma_{\text{A}}/d_{\text{A}}$ range from 0.01 to 0.07 and those for $\sigma_{\text{B}}/d_{\text{B}}$ range from 0.10 to 0.16, indicating

Table 3. Lamellar Fitting Parameters for Fits of $I_{\text{lam}}(q) + I_{\text{A,fluc}}(q)$ and $I_{\text{lam}}(q)$ to $I(q)$ for Blend OC25 at 30 °C

	$I_{\text{lam}}(q) + I_{\text{A,fluc}}(q)$	$I_{\text{lam}}(q)$
$A \times 10^{10}$ (cm^{-1} nm^{-4})	5.85	8.50
$\phi_{\text{A,TOT}}$	0.396	0.183
σ_{A} (nm)	3.01	2.85
σ_{B} (nm)	4.86	9.44
d (nm)	64.1	62.1

Table 4. SANS Lamellar Fitting Parameters for Blend OC10 at Selected Temperatures and Two Different Annealing Conditions

	190 °C anneal			90 °C anneal	
T (°C)	110	118	122	30	110
$A \times 10^{10}$ (cm^{-1} nm^{-4})	3.592	3.49	3.32	5.10	2.53
$\phi_{\text{A,TOT}}$	0.412	0.356	0.344	0.431	0.359
σ_{A} (nm)	4.53	4.94	6.18	0.969	5.45
σ_{B} (nm)	10.4	10.1	14.7	6.38	12.2
d (nm)	72.6	84.0	90.2	59.9	74.7

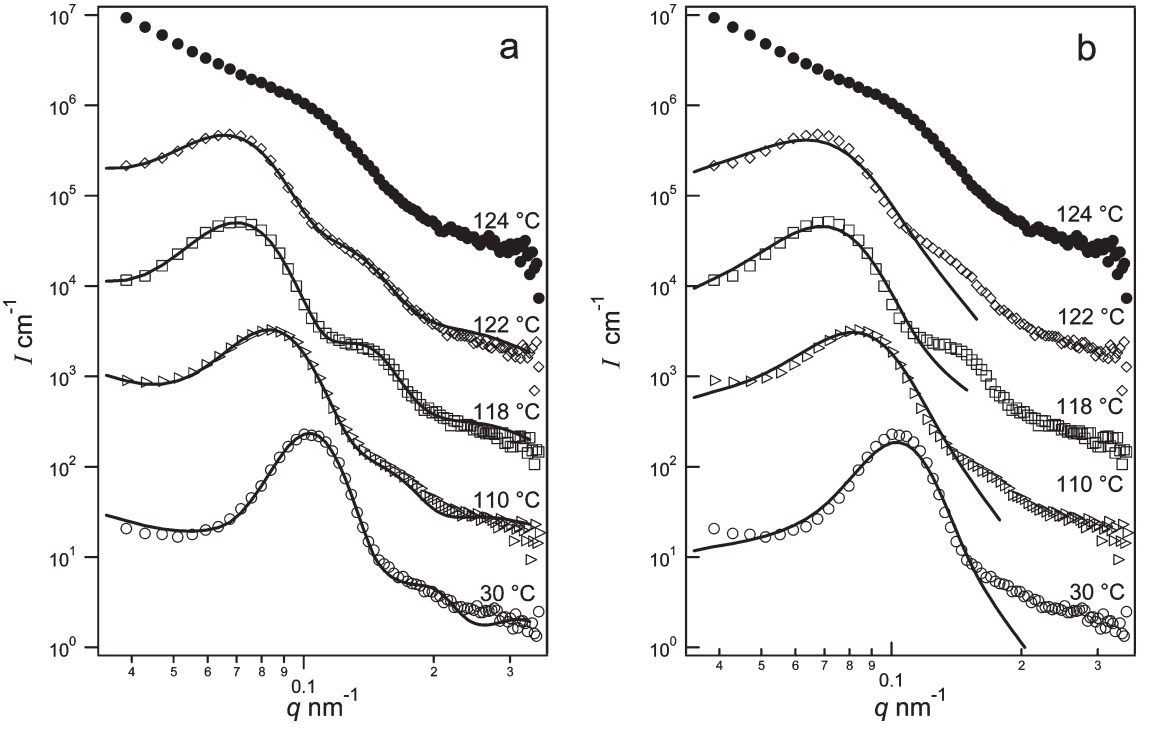

Figure 4. SANS intensity, I, versus scattering vector, q, for blend OC10 at selected temperatures (markers) and solid-line fits to the data for (a) $I_{\text{lam}}(q)$ and (b) $I_{\mu\text{E}}(q)$. Intensity profiles in both figures were shifted for clarity: 6.0×10^6 cm^{-1} (124 °C), 4.4×10^6 cm^{-1} (122 °C), 3.0×10^6 cm^{-1} (116 °C), 1.6×10^6 cm^{-1} (110 °C), and 0 cm^{-1} (30 °C).

Table 5. Teubner−Strey Fitting Parameters for Blend OC10 at Selected Temperatures[a]

	90 °C anneal	190 °C anneal		
T (°C)	30	110	116	122
a (cm)	0.309	0.099	0.062	0.037
$b \times 10^{-5}$ (cm nm^{-2})	−5.51	−2.60	−2.09	−1.44
$c \times 10^{-11}$ (cm nm^{-4})	2.52	1.85	1.95	1.64

[a] The annealing conditions are noted at the top of the table.

that the lamellar thicknesses vary around 10−20% in the sample. We do not ascribe any particular significance to the fitted value of C, merely noting that it contains contributions from the scattering contrast and the number of lamellar stacks within the scattering volume.

The above analysis was repeated on all of the blends listed in Table 2. The data from 30 to 120 °C were consistent with the $I_{lam}(q)$ fits for all blends. The ranges of parameters obtained from the fits are listed in Table 2. For blends that were run twice, the fitting parameters from the second thermal history were found to be within the same ranges as those for the first run. In all cases, the fits with $I_{lam}(q)$ were significantly better than those with $I_{\mu E}(q)$.

In our previous studies on A/B/A−C mixtures,[21−29] we assumed that samples with peaks that could not be fit with $I_{\mu E}(q)$ were lamellar. The main advance that we have made here is to show that scattering profiles that are inconsistent with $I_{\mu E}(q)$ fits are actually consistent with $I_{lam}(q)$ fits. This is especially important in cases where higher order peaks are not evident in the scattering profiles. We note in passing that the effect of instrument resolution is significant, and quantitative agreement between the model and experiments is not obtained without accounting for this effect.

Theoretical predictions of equilibrium domain spacings were carried out using one-dimensional SCFT calculations. The equations used in these calculations and our methods for solving the equations are given in ref 23. The program used was written by Dr. Benedict Reynolds. Inputs to the SCFT calculations include the binary Flory−Huggins parameters describing monomer−monomer interactions and the statistical segment length of each species (homopolymers and blocks). We use previously published values of these parameters[27] summarized in footnote 66. The Helmholtz free energy density was calculated for a range of domain spacings, and the equilibrium domain spacing was determined from the minimum in the free energy curve. Figure 5 compares the SCFT predictions for the equilibrium domain spacing in blends OC10, TB0.6, and OC50 with the domain spacings measured using SANS. There is quantitative agreement between the measured and predicted data. At the extremities of the ϕ_A range studied (OC10 and OC50) the domain spacing changes monotonically with temperature: increasing for OC10 and decreasing for OC50. Trends are not monotonic for mid-range values of ϕ_A where the system is transitioning between thermal swelling of the lamellar domains and thermal deswelling. For blend TB0.6 we also show the lamellar domain spacing determined by fitting a Gaussian curve to the primary scattering peak, q^*, and defining $d = 2\pi/q^*$. The domain spacings calculated using this method vary by 2−5 nm from those determined by fitting a lamellar structure factor.

To determine the underpinnings of the swelling and deswelling behavior seen in Figure 5, we examine the concentration profiles of the components calculated by SCFT. Parts a and b of Figure 6 show the concentration of the components in our blends as a function of reduced distance, z/d, for OC10 at 30 and 130 °C, respectively. The B-rich domain, which is the larger domain in this blend, has a more uniform composition at 30 °C than at 130 °C (the highest temperature where the SCFT calculations converged). This can be seen by the distinct valley in the C-block concentration profile in the vicinity of $z/d = 0.5$ and the sharp peak in the B concentration in that region. This implies a transition from the wet brush regime at 30 °C to a dry brush regime at 130 °C. The driving force for this transition is clear. At low temperatures, χ_{BC} is negative, and this promotes mixing between the B homopolymer and the C-block. This favorable interaction diminishes in magnitude with increasing temperature, resulting in an expulsion of the B chains from the brush. The domain size is smaller in the wet brush regime where the B−C copolymer is an effective surfactant. OC10 domains thus swell with increasing temperature.

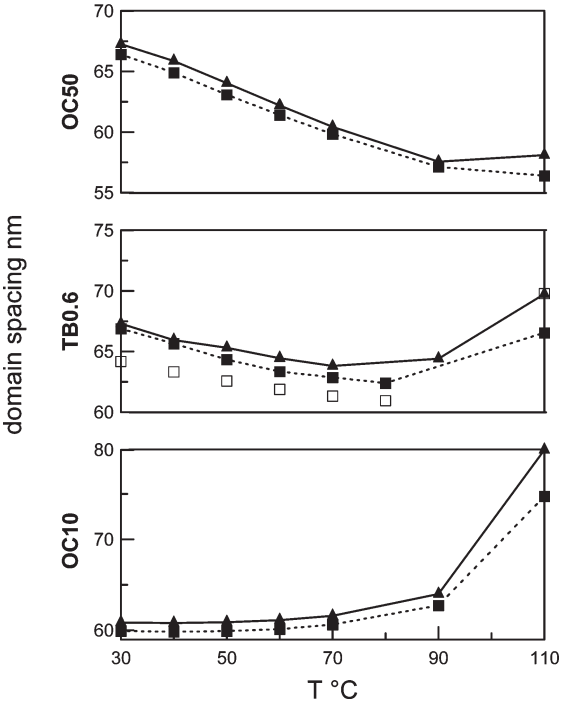

Figure 5. Lamellar domain spacings for selected blends across the experimental range of temperatures. Values obtained from fitting the SANS data with the lamellar structure factor (■) are compared to values calculated using SCFT (▲). For blend TB0.6, the lamellar domain spacing is also shown as calculated by $d = 2\pi/q^*$, where q^* is determined from a Gaussian fit to the primary scattering peak (□). Lines are drawn between the data points for visual clarity. Error bars are smaller than the symbol size.

Parts c and d of Figure 6 show the concentration profiles for OC50 at 30 and 98 °C, respectively. The A-rich domain, which is the larger domain in this blend, has a more uniform composition at 98 °C than at 30 °C. Note that at 30 °C the A homopolymer chains are being expelled from the A-block brush in spite of the fact that $N_A/N_{A-C} = 0.17$. In this case, increasing temperature causes a dry brush to wet brush transition and concomitant deswelling of the lamellae. Since the interactions between the A-block and the A-homopolymer are entropic (to a very good approximation, ignoring the effect of deuteration on thermodynamics),[3,35,36,41] the observed temperature dependence must arise from the other intermolecular interactions in the system. The mixing of A-homopolymer chains seen in both A-rich and B-rich domains is driven by a decrease in χ_{AB} and χ_{AC} with increasing temperature.

The SCFT calculations show the limitations of our scattering analysis. In particular, the assumption of ideal mixing of deuterated and hydrogenated A chains ignores the presence of concentration fluctuations due to the presence of B and C chains in the A-rich microphase. It may be possible to include the effects of

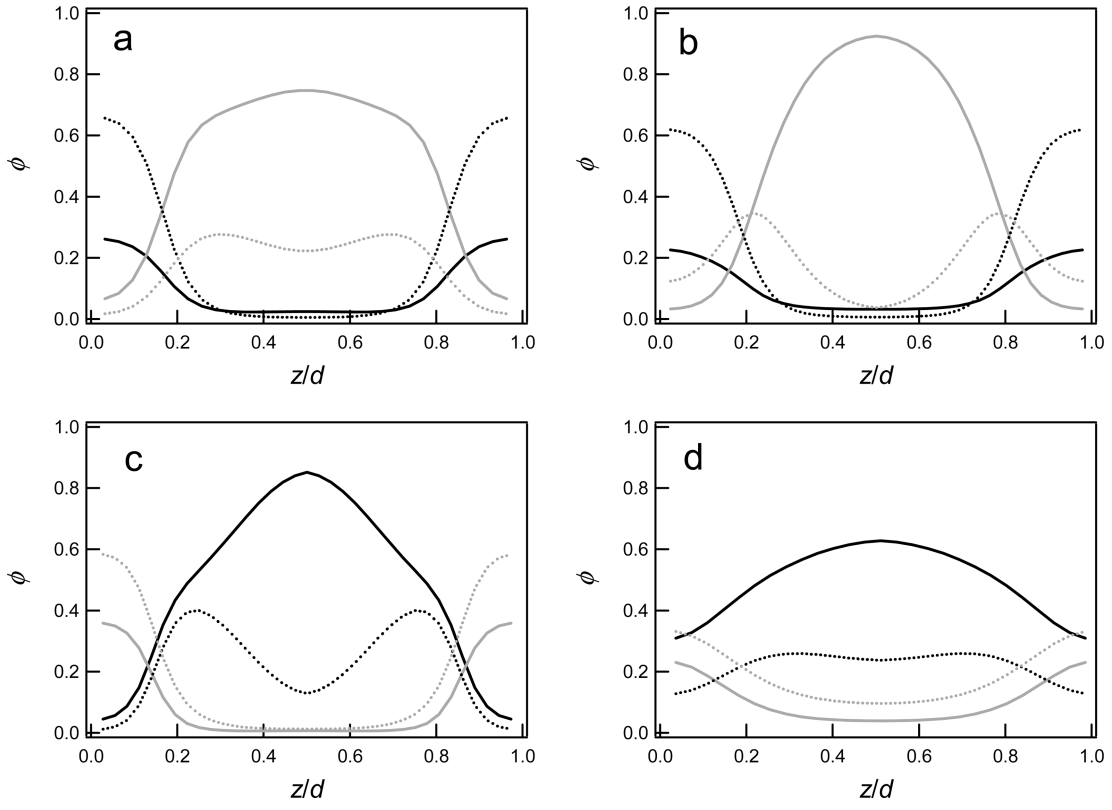

Figure 6. SCFT lamellar concentration profiles for selected blends at selected temperatures: (a) OC10 at 30 °C, (b) OC10 at 130 °C, (c) OC50 at 30 °C, (d) OC50 at 98 °C. The volume fraction of each component is shown against z/d, the dimensionless distance through a single domain spacing. Homopolymer A is shown in solid black, homopolymer B is solid gray, block A is a broken black line, and block C is a broken gray line.

these fluctuations but this is outside the scope of the present paper. One may also question the validity of adding fluctuation and lamellar contributions to scattering.

The results of the SCFT calculations are now compared with experimental results based on fits of the SANS profiles to the lamellar structure factor (eq 4).[3,35,36,41] We define the interface between A-rich and B-rich domains to be located at the z value that is an arithmetic average of the z locations corresponding to the midpoint values in the concentration profiles of A and B, respectively. The distance between adjacent interfaces across an A-rich domain is z_A, allowing us to define $\phi_{A\text{-dom}} = z_A/d$. We define the interfacial width for each species following the work of Shull et al.:[36,41]

$$\sigma_i = \frac{1}{2}(\phi_{i,\max} - \phi_{i,\min})\left[\left.\frac{\partial \phi_i}{\partial z}\right|_{z_{avg}}\right]^{-1} \quad (9)$$

The index i is either species A or B, and $\phi_{i,\max}$ and $\phi_{i,\min}$ are the maximum and minimum volume fractions of the components.

In Figure 7a−d we compare the SCFT predictions of $\phi_{A\text{-dom}}$, σ_A, σ_B, and d at 30 °C with experimental measurements. The values for $\phi_{A\text{-dom}}$ in Figure 7a are plotted against the bulk fraction of component A, $\phi_{A,TOT}$. The line with slope of unity represents the expectation $\phi_{A\text{-dom}} = \phi_{A,TOT}$ in the limit of highly incompatible A/B mixtures. SCFT predicts that $\phi_{A\text{-dom}}$ increases continuously with increasing $\phi_{A,TOT}$. In contrast, $\phi_{A\text{-dom}}$ obtained from fitting SANS data shows more of a steplike behavior, changing dramatically in the vicinity of $\phi_{A,TOT} = 0.6$ (between blends TB0.6 and OC40). The trends observed for both SCFT and experiments were relatively invariant with temperature. Parts b and c of Figure 7 show the dependence of σ_A and σ_B, respectively, on ϕ_A. Both SCFT and SANS indicate that the width of the A-interface increases with increasing ϕ_A. On the other hand, SANS results indicate that the width of the B-interface decreases with ϕ_A while SCFT predicts that the width of the B-interface is nearly independent of ϕ_A. Figure 7d shows that there is relatively good agreement between the equilibrium domain spacings predicted by SCFT and those measured experimentally. We are not sure if the lack of quantitative agreement between theory and experiment seen in Figure 7 is due to a lack of uniqueness of the fitted parameters obtained from the SANS profiles or due to complexity of the thermodynamics of A/B/A−C mixtures that go beyond the simple mean-field theories used here.

SCFT calculations were performed for each blend over a range of temperatures to determine the stability window of the lamellar phase. The predicted location of the phase boundary is the temperature T_{SCFT}, above which the calculated free energy density changes monotonically with domain spacing and does not exhibit a minimum. At temperatures above T_{SCFT} we use RPA to distinguish between one-phase and phase-separated systems. The SANS profiles from homogeneous blends were calculated using the multicomponent random phase approximation (RPA)[67,68] using the same parameters as those used in the SCFT calculations.[66] A homogeneous phase is predicted where the RPA calculations give SANS profiles without singularities. Outside the homogeneous window, RPA calculations contain poles indicating either microphase or macrophase separation. The phase behavior predicted using both the RPA and SCFT is compared to the experimentally determined behavior in Figure 8.

The experimental data are shown in Figure 8 with markers indicating the temperatures at which the onset of macrophase separation was observed by SANS. The region for which RPA predicts a homogeneous phase is shown along with the region for which SCFT predicts lamellae. There is a small region of overlap between the homogeneous region predicted by RPA and

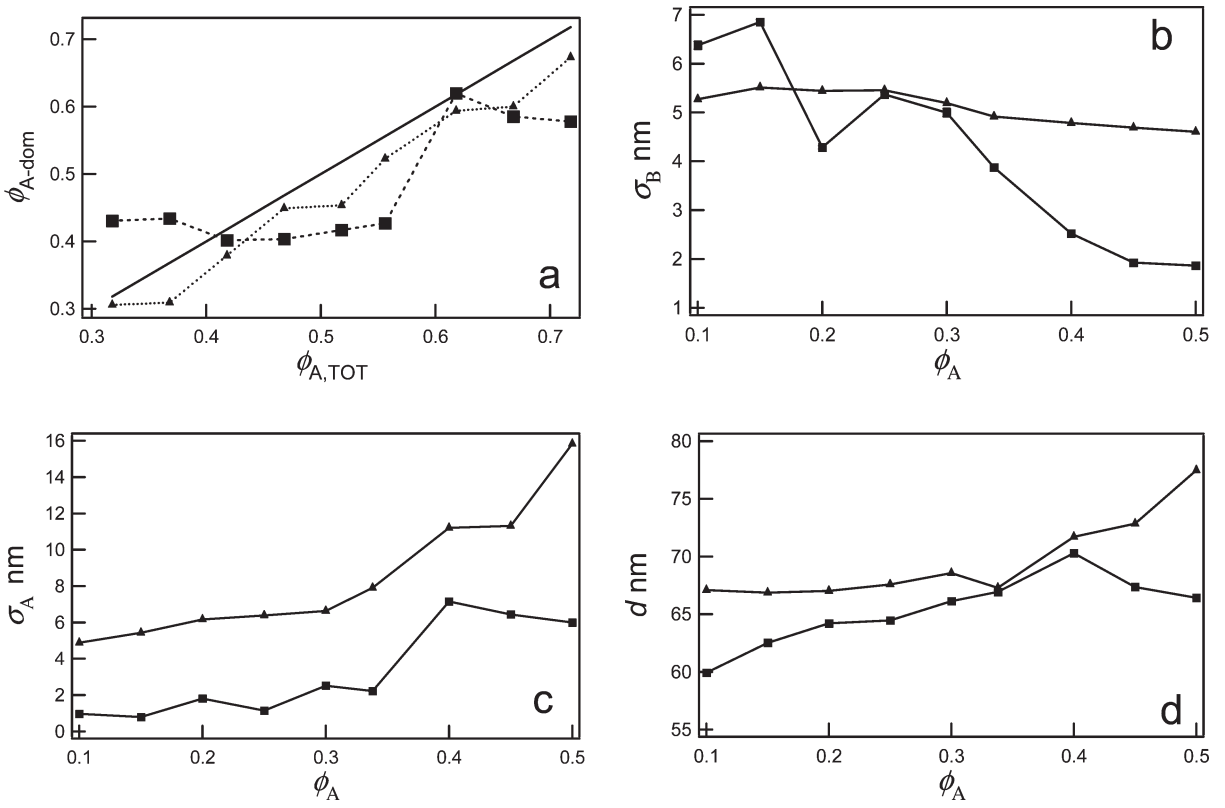

Figure 7. Comparison of parameters at 30 °C calculated using SCFT (▲) with those obtained by fitting the SANS data with a lamellar structure factor (■). (a) $\phi_{A\text{-dom}}$ is plotted against the bulk fraction of component A in each blend, $\phi_{A,TOT}$. The solid line indicates $x = y$. (b) Interfacial widths of the microdomains, σ_A and σ_B, are plotted against ϕ_A for each blend. (c) Domain spacing, d, is plotted against ϕ_A for each blend. Error bars for all data fall within the symbol size.

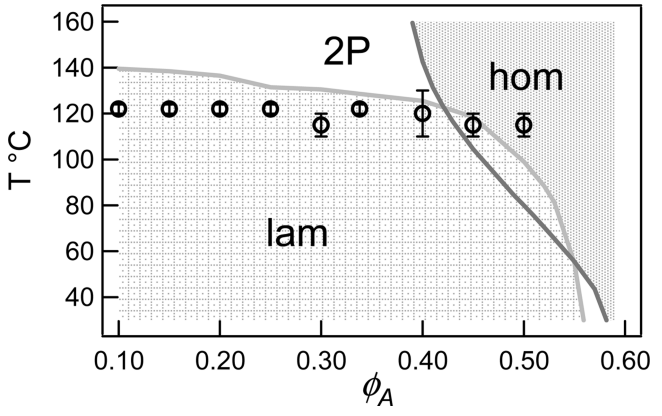

Figure 8. Phase transition temperature as a function of volume fraction of A homopolymer, ϕ_A. Markers represent the experimentally determined transitions from lamellae (lam) to macrophase separation (2P). The uniformly shaded region labeled "hom" represents phase space where the RPA predicts a single homogeneous phase, and the checkered region labeled "lam" is phase space where SCFT predicts a lamellar phase.

microphase separation predicted by SCFT. It is likely due to errors introduced in the coarse-graining used for the SCFT calculations. Figure 8 shows that the experimentally observed transitions from lamellae to macrophase separation are in quantitative agreement with SCFT/RPA calculations. The theoretical analysis predicts the existence of homogeneous windows for blends OC45 and OC50, but these were not seen in experiments. It is evident from Figure 8 that varying ϕ_A from 0.1 to 0.5 has virtually no effect on the phase behavior of our A/B/A−C system. This behavior is very surprising as both the geometry of microphases and stability windows are usually strong functions of composition.[7,13,17,57,69]

Conclusion

We have used SANS to determine the phase behavior in a series of ternary A/B/A−C blends where ϕ_A was systematically varied from 0.10 to 0.50. This is the first study of A/B/A−C blends wherein the A−C copolymer is added to off-critical A/B mixtures. Surprisingly, all blends exhibited the same phase behavior: lamellae at low temperatures and macrophase separation at high temperatures. The transition temperature was above 119 ± 4 °C, regardless of ϕ_A. Detailed fitting of the lamellar structure factor to the low-temperature SANS data provided quantitative insight into the nature of the A-rich and B-rich domains. The size and widths of these domains were compared with SCFT predictions based on χ parameters and statistical segment lengths measured independently from experiments on binary homopolymer blends. The stability window of the lamellae formed in off-critical A/B/A−C mixtures was in reasonable agreement with predictions based on SCFT and RPA.

Acknowledgment. We acknowledge The Dow Chemical Company for providing the primary support for this work and Dr. T. H. Kalanthar for guidance and helpful discussions. A.J.N. was also supported by the Tyco Fellowship. We acknowledge the support of the National Institute of Standards and Technology, U.S. Department of Commerce, in providing the neutron research facilities used in this work. This work utilized facilities supported in part by the National Science Foundation under Agreement DMR-0454672.

References and Notes

(1) Bates, F. S. *Science* **1991**, *251*, 898–905.
(2) Balsara, N. P.; Jonnalagadda, S. V.; Lin, C. C.; Han, C. C.; Krishnamoorti, R. *J. Chem. Phys.* **1993**, *99*, 10011–10020.

(3) Shull, K. R.; Kellock, A. J.; Deline, V. R.; Macdonald, S. A. *J. Chem. Phys.* **1992**, *97*, 2095–2104.
(4) Schwahn, D.; Mortensen, K.; Frielinghaus, H.; Almdal, K.; Kielhorn, L. *J. Chem. Phys.* **2000**, *112*, 5454–5472.
(5) Schwahn, D.; Mortensen, K.; Frielinghaus, H.; Almdal, K. *Physica B* **2000**, *276*, 353–354.
(6) Schwahn, D. *Phase Behav. Polym. Blends* **2005**, *183*, 1–61.
(7) Schwahn, D.; Willner, L. *Appl. Phys. A: Mater. Sci. Process.* **2002**, *74*, S358–S360.
(8) Morkved, T. L.; Stepanek, P.; Krishnan, K.; Bates, F. S.; Lodge, T. P. *J. Chem. Phys.* **2001**, *114*, 7247–7259.
(9) Morkved, T. L.; Chapman, B. R.; Bates, F. S.; Lodge, T. P.; Stepanek, P.; Almdal, K. *Faraday Discuss.* **1999**, *112*, 335–350.
(10) Hu, W. C.; Koberstein, J. T.; Lingelser, J. P.; Gallot, Y. *Macromolecules* **1995**, *28*, 5209–5214.
(11) Hillmyer, M. A.; Maurer, W. W.; Lodge, T. P.; Bates, F. S.; Almdal, K. *J. Phys. Chem. B* **1999**, *103*, 4814–4824.
(12) Bates, F. S.; Maurer, W. W.; Lipic, P. M.; Hillmyer, M. A.; Almdal, K.; Mortensen, K.; Fredrickson, G. H.; Lodge, T. P. *Phys. Rev. Lett.* **1997**, *79*, 849–852.
(13) Bates, F. S.; Maurer, W.; Lodge, T. P.; Schulz, M. F.; Matsen, M. W.; Almdal, K.; Mortensen, K. *Phys. Rev. Lett.* **1995**, *75*, 4429–4432.
(14) Adedeji, A.; Hudson, S. D.; Jamieson, A. M. *Macromolecules* **1996**, *29*, 2449–2456.
(15) Adedeji, A.; Jamieson, A. M.; Hudson, S. D. *Macromolecules* **1995**, *28*, 5255–5261.
(16) Washburn, N. R.; Lodge, T. P.; Bates, F. S. *J. Phys. Chem. B* **2000**, *104*, 6987–6997.
(17) Corvazier, L.; Messe, L.; Salou, C. L. O.; Young, R. N.; Fairclough, J. P. A.; Ryan, A. J. *J. Mater. Chem.* **2001**, *11*, 2864–2874.
(18) Ho, R. M.; Chiang, Y. W.; Lin, C. C.; Bai, S. J. *Macromolecules* **2002**, *35*, 1299–1306.
(19) Zhou, N.; Bates, F. S.; Lodge, T. P. *Nano Lett.* **2006**, *6*, 2354–2357.
(20) Meuler, A. J.; Hillmyer, M. A.; Bates, F. S. *Macromolecules* **2009**, *42*, 7221–7250.
(21) Lee, J. H.; Ruegg, M. L.; Balsara, N. P.; Zhu, Y. Q.; Gido, S. P.; Krishnamoorti, R.; Kim, M. H. *Macromolecules* **2003**, *36*, 6537–6548.
(22) Lee, J. H.; Balsara, N. P.; Chakraborty, A. K.; Krishnamoorti, R.; Hammouda, B. *Macromolecules* **2002**, *35*, 7748–7757.
(23) Reynolds, B. J.; Ruegg, M. L.; Balsara, N. P.; Radke, C. J.; Shaffer, T. D.; Lin, M. Y.; Shull, K. R.; Lohse, D. J. *Macromolecules* **2004**, *37*, 7401–7417.
(24) Ruegg, M. L.; Reynolds, B. J.; Lin, M. Y.; Lohse, D. J.; Balsara, N. P. *Macromolecules* **2006**, *39*, 1125–1134.
(25) Ruegg, M. L.; Reynolds, B. J.; Lin, M. Y.; Lohse, D. J.; Balsara, N. P. *Macromolecules* **2007**, *40*, 1207–1217.
(26) Ruegg, M. L.; Reynolds, B. J.; Lin, M. Y.; Lohse, D. J.; Krishnamoorti, R.; Balsara, N. P. *Macromolecules* **2007**, *40*, 355–365.
(27) Robertson, M. L. Ph.D. Dissertation, University of California, Berkeley, Berkeley, CA, 2006.
(28) Wanakule, N. S.; Nedoma, A. J.; Robertson, M. L.; Fang, Z.; Jackson, A.; Garetz, B. A.; Balsara, N. P. *Macromolecules* **2008**, *41*, 471–477.
(29) Nedoma, A. J.; Lai, P.; Jackson, A.; Robertson, M. L.; Wanakule, N. S.; Balsara, N. P. *Macromolecules* **2010**, *43*, 3549–3555.
(30) Noolandi, J.; Hong, K. M. *Macromolecules* **1984**, *17*, 1531–1537.
(31) Leibler, L. *Makromol. Chem., Macromol. Symp.* **1988**, *16*, 1–17.
(32) Broseta, D.; Fredrickson, G. H. *J. Chem. Phys.* **1990**, *93*, 2927–2938.
(33) Kao, C. H. R.; Delacruz, M. O. *J. Chem. Phys.* **1990**, *93*, 8284–8293.
(34) Winey, K. I.; Thomas, E. L.; Fetters, L. J. *J. Chem. Phys.* **1991**, *95*, 9367–9375.
(35) Winey, K. I.; Thomas, E. L.; Fetters, L. J. *Macromolecules* **1991**, *24*, 6182–6188.
(36) Shull, K. R.; Winey, K. I. *Macromolecules* **1992**, *25*, 2637–2644.
(37) Winey, K. I.; Thomas, E. L.; Fetters, L. J. *Macromolecules* **1992**, *25*, 2645–2650.
(38) Semenov, A. N. *Macromolecules* **1992**, *25*, 4967–4977.
(39) Lerczak, J.; Schick, M.; Gompper, G. *Phys. Rev. A* **1992**, *46*, 985–993.
(40) Semenov, A. N. *Macromolecules* **1993**, *26*, 2273–2281.
(41) Shull, K. R.; Mayes, A. M.; Russell, T. P. *Macromolecules* **1993**, *26*, 3929–3936.
(42) Matsen, M. W.; Schick, M. *Macromolecules* **1994**, *27*, 2316–2318.
(43) Muller, M.; Schick, M. *J. Chem. Phys.* **1996**, *105*, 8885–8901.
(44) Kielhorn, L.; Muthukumar, M. *J. Chem. Phys.* **1997**, *107*, 5588–5608.
(45) Janert, P. K.; Schick, M. *Macromolecules* **1998**, *31*, 1109–1113.
(46) Duchs, D.; Ganesan, V.; Fredrickson, G. H.; Schmid, F. *Macromolecules* **2003**, *36*, 9237–9248.
(47) Cavallo, A.; Muller, M.; Binder, K. *Macromolecules* **2006**, *39*, 9539–9550.
(48) Thompson, R. B.; Matsen, M. W. *J. Chem. Phys.* **2000**, *112*, 6863–6872.
(49) Kahlweit, M.; Strey, R. *Angew. Chem., Int. Ed. Engl.* **1985**, *24*, 654–668.
(50) Kahlweit, M.; Strey, R.; Firman, P.; Haase, D. *Langmuir* **1985**, *1*, 281–288.
(51) Kahlweit, M.; Strey, R.; Haase, D.; Firman, P. *Langmuir* **1988**, *4*, 785–790.
(52) Kaler, E. W.; Labourt-Ibarre, M. *Abstr. Pap. Am. Chem. Soc.* **2002**, *224*, 261–COLL.
(53) Flory, P. I. *J. Chem. Phys.* **1942**, *10*, 51–61.
(54) Huggins, M. L. *J. Phys. Chem.* **1942**, *46*, 151–158.
(55) Nedoma, A. J.; Robertson, M. L.; Wanakule, N. S.; Balsara, N. P. *Macromolecules* **2008**, *41*, 5773–5779.
(56) Note: certain commercial equipment, instruments, materials, and suppliers are identified in this paper to foster understanding. Such identification does not imply recommendation or endorsement by the National Institute of Standards and Technology, nor does it imply that the materials or equipment identified are necessarily the best available for the purpose.
(57) Holyst, R.; Schick, M. *J. Chem. Phys.* **1992**, *96*, 7728–7737.
(58) Balsara, N. P.; Lohse, D. J.; Graessley, W. W.; Krishnamoorti, R. *J. Chem. Phys.* **1994**, *100*, 3905–3910.
(59) Kline, S. R. *J. Appl. Crystallogr.* **2006**, *39*, 895.
(60) Balsara, N. P.; Dai, H. J. *J. Chem. Phys.* **1996**, *105*, 2942–2945.
(61) Jeon, H. S.; Lee, J. H.; Balsara, N. P. *Macromolecules* **1998**, *31*, 3328–3339.
(62) Strey, R. *Colloid Polym. Sci.* **1994**, *272*, 1005–1019.
(63) Nallet, F.; Laversanne, R.; Roux, D. *J. Phys. II* **1993**, *3*, 487–502.
(64) Hosemann, R.; Bagchi, S. N. *Direct Analysis of Diffraction by Matter*; North-Holland: Amsterdam, 1962.
(65) Roe, R.-J. *Methods of X-ray and Neutron Scattering in Polymer Science*; Oxford University Press: New York, 2000.
(66) Note: temperatures are in K: $\chi_{AB} = 0.00034 + 3.94/T - 817/T^2$; $\chi_{AC} = 0.00209 - 1.18/T + 747/T^2$; $\chi_{BC} = -0.00085 + 6.87/T - 2480/T^2$. Statistical Segment lengths: $l_A = 0.55$ nm; $l_B = 0.58$ nm; $l_C = 0.75$ nm.
(67) deGennes, P. G. In *Scaling Concepts in Polymer Physics*; Cornell University Press: Ithaca, NY, 1979; p 109.
(68) Benoit, H.; Benmouna, M.; Wu, W. L. *Macromolecules* **1990**, *23*, 1511–1517.
(69) Ellison, C. J.; Meuler, A. J.; Qin, J.; Evans, C. M.; Wolf, L. M.; Bates, F. S. *J. Phys. Chem. B* **2009**, *113*, 3726–3737.